





## Article

# Cosmogenic Exposure Dating ( $^{36}\text{Cl}$ ) of Landforms on Jan Mayen, North Atlantic, and the Effects of Bedrock Formation Age Assumptions on $^{36}\text{Cl}$ Ages

Johanna Anjar <sup>1,\*</sup> , Naki Akçar <sup>2</sup> , Eiliv A. Larsen <sup>3</sup>, Astrid Lyså <sup>3</sup>, Shasta Marrero <sup>4</sup> , Nasim Mozafari <sup>2</sup>  and Christof Vockenhuber <sup>5</sup>

<sup>1</sup> Department of Natural Sciences and Environmental Health, University of South-Eastern Norway, Gullbringvegen 36, 3800 Bø, Norway

<sup>2</sup> Institute of Geological Sciences, University of Bern, Baltzerstrasse 1-3, 3012 Bern, Switzerland; akcar@geo.unibe.ch (N.A.); nasim.mozafari@geo.unibe.ch (N.M.)

<sup>3</sup> Geological Survey of Norway, P.O. Box 6315, Torgarden, 7491 Trondheim, Norway; eiliv.larsen@ngu.no (E.A.L.); astrid.lysa@ngu.no (A.L.)

<sup>4</sup> School of Earth and Environmental Sciences, Cardiff University, Main Building, Park Place, Cardiff CF10 3AT, UK; marreros@cardiff.ac.uk

<sup>5</sup> Laboratory of Ion Beam Physics, ETH Zürich, 8093 Zürich, Switzerland; vockenhuber@phys.ethz.ch

\* Correspondence: johanna.anjar@usn.no



**Citation:** Anjar, J.; Akçar, N.; Larsen, E.A.; Lyså, A.; Marrero, S.; Mozafari, N.; Vockenhuber, C. Cosmogenic Exposure Dating ( $^{36}\text{Cl}$ ) of Landforms on Jan Mayen, North Atlantic, and the Effects of Bedrock Formation Age Assumptions on  $^{36}\text{Cl}$  Ages. *Geosciences* **2021**, *11*, 390. <https://doi.org/10.3390/geosciences11090390>

Academic Editors: Ángel Rodés and Jesus Martinez-Frias

Received: 14 July 2021

Accepted: 10 September 2021

Published: 15 September 2021

**Publisher's Note:** MDPI stays neutral with regard to jurisdictional claims in published maps and institutional affiliations.



**Copyright:** © 2021 by the authors. Licensee MDPI, Basel, Switzerland. This article is an open access article distributed under the terms and conditions of the Creative Commons Attribution (CC BY) license (<https://creativecommons.org/licenses/by/4.0/>).

**Abstract:** Jan Mayen is a small volcanic island situated 550 km north of Iceland. Glacial sediments and landforms are relatively common on the island but, so far, only a few of them have been dated. In this study, we present and discuss 89  $^{36}\text{Cl}$  dates of primarily glacial and volcanic events on Jan Mayen. Calculations of sample exposure ages were complicated by young exposure ages, young rock formation age, and high native Cl contents, leading to updates in CRONUScalc to enable accurate exposure age calculations. The samples provide good evidence against an equilibrium assumption when subtracting background production (e.g.,  $^{36}\text{Cl}$  produced by neutron capture from fission of U or Th) for samples on young bedrock, with younger exposure ages most significantly affected. Exposure ages were calculated with a range of assumptions of bedrock formation ages appropriate for Jan Mayen, including the assumption that the rock formation age equaled the exposure age (i.e., the youngest age it could possibly have), and we found that although the effect on most of the ages was small, the calculated ages of 25 of the samples increased by more than 1 standard deviation from the age calculated assuming equilibrium background production, with a maximum deviation of 6.1 ka. Due to the very young bedrock on Jan Mayen, we consider the nonequilibrium ages to be the most reliable ages from the island and conclude that large-scale deglaciation on the south and central, lower-lying, parts of the island, started around 20 ka and lasted until ~7 ka. On northern Jan Mayen, the slopes of the 2277 m high stratovolcano Beerenberg are currently partly glaciated; however, outside of the Little Ice Age moraines, all but two samples give ages between 14 and 5.7 ka.

**Keywords:** cosmogenic surface exposure dating;  $^{36}\text{Cl}$ ; Jan Mayen; background production

## 1. Introduction

Jan Mayen is a small volcanic island. Its isolated position 550 km north of Iceland and 450 km east of Greenland in the Norwegian–Greenland Sea (Figure 1) makes it an interesting location for investigations of the climate history in the North Atlantic. A research campaign to reconstruct the glaciation and climate history of the island was therefore started in 2014 [1,2]. As part of that campaign, 89 samples for cosmogenic nuclide exposure age dating ( $^{36}\text{Cl}$ ) were collected with the aim of dating glacial and volcanic events on the island.

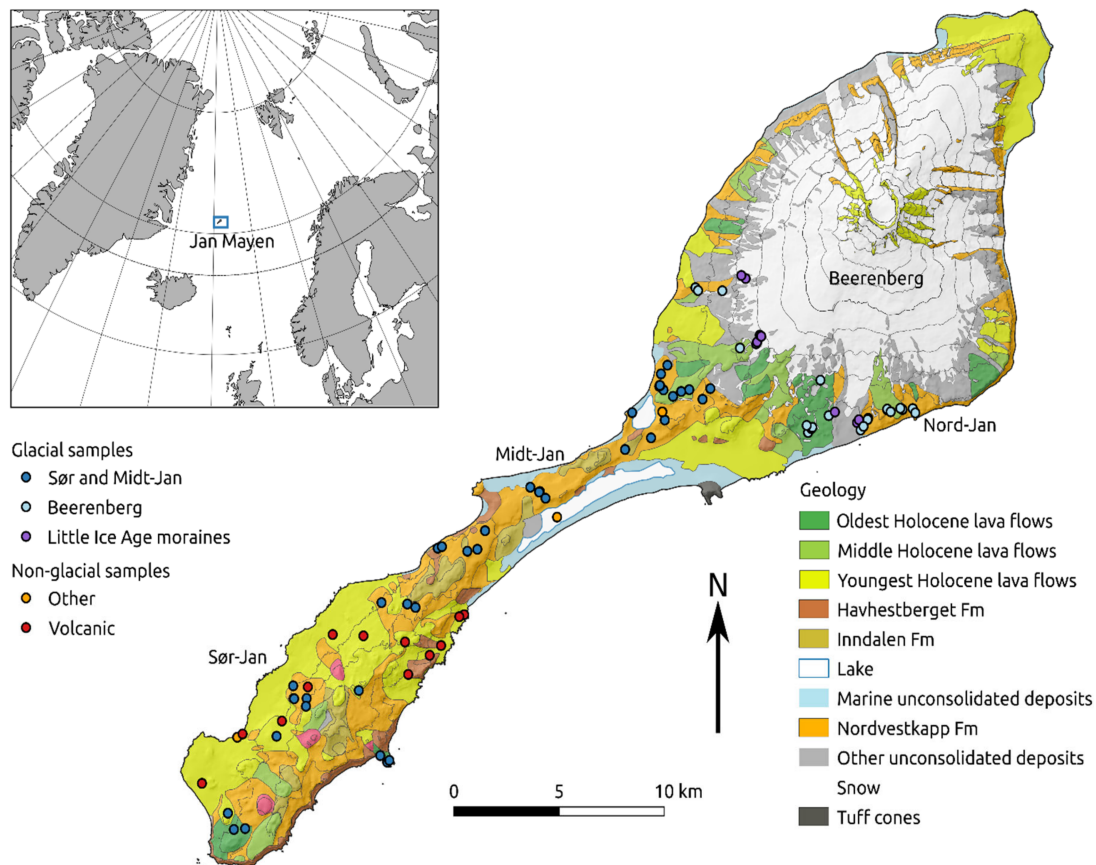


**Figure 1.** Geological map of Jan Mayen [3]. The different map unit colors indicate the different ages of the lava flows. Sample locations are marked by circles and the colors indicate the sample setting: dark blue indicates samples from glacial settings on south and central Jan Mayen; light blue indicates glacial samples from the slopes of Beerenberg; purple indicates samples from the young Little Ice Age (LIA) moraines; red indicates samples that are related to volcanism; samples that are unrelated to deglaciation or volcanism are classified as “other” and indicated in orange.

Exposure dating in an active volcanic landscape comes with its own challenges. In addition to being created through cosmogenic processes,  $^{36}\text{Cl}$  is also created when  $^{35}\text{Cl}$  absorbs neutrons produced from fission and (alpha, n) reactions, including uranium and thorium decay (for simplicity, all these reactions are referred to as “background production” herein). These neutron capture reactions occur in both the thermal and epithermal energy ranges [4], and the general formula is provided in Equation (1). The total  $^{36}\text{Cl}$  atoms attributed to background production ( $N_{36, \text{background}}$ ) for any given sample is dependent on the formation age of the rock ( $t_{\text{form}}$ ) and the composition of the sample (through the calculation of the total background production rate,  $P_{36, \text{background}}$ , in  $^{36}\text{Cl}$  atoms  $\text{g}^{-1} \text{y}^{-1}$ ). The elemental composition of the sample determines both the creation rate of low-energy neutrons and the total absorption of those neutrons by  $^{35}\text{Cl}$  and other elements present in the sample. Although the timescale for background production is dependent only on the half-life of  $^{36}\text{Cl}$  ( $t_{1/2}$ , related to the decay constant,  $\lambda_{36}$ , through  $\lambda_{36} = \ln(2)/t_{1/2}$ ), elemental composition determines the magnitude of the background production. Full details of the reactions considered in these calculations and the effects of sample composition can be found in Gosse and Phillips (2001) [4] and Marrero et al. (2016a) [5].

$$N_{36, \text{background}} = P_{36, \text{background}} \left[ \frac{1 - \exp(-t_{\text{form}} \lambda_{36})}{\lambda_{36}} \right] \quad (1)$$



To estimate the cosmogenically produced  $^{36}\text{Cl}$  in the sample, the background production is subtracted from the measured  $^{36}\text{Cl}$  concentration. For many samples, the rock formation age is sufficiently old that production of  $^{36}\text{Cl}$  from background processes balances radioactive decay (Figure 2, see also Equation (1) as  $t_{\text{form}}$  becomes large), i.e., equilibrium conditions have been achieved. Standard methods for age calculations assume that this equilibrium condition has been reached for all samples [5,6]. However, the assumption that the background production has had time to reach equilibrium is unlikely to be true in areas with young volcanic rocks [7–9], such as Jan Mayen [1,2,10]. If equilibrium conditions are assumed incorrectly, the background production subtraction will be too large, resulting in an exposure age that is too young. This incorrect equilibrium assumption is most likely to affect samples that meet three criteria: short exposure duration, young rock formation age, and susceptible composition (high in both native Cl and neutron-producing elements such as uranium and thorium). Although there are other models that do not make this assumption (e.g., Schimmelpfennig et al. (2009) [7]), they require manual iteration and were not available for a range of production rate scaling models.

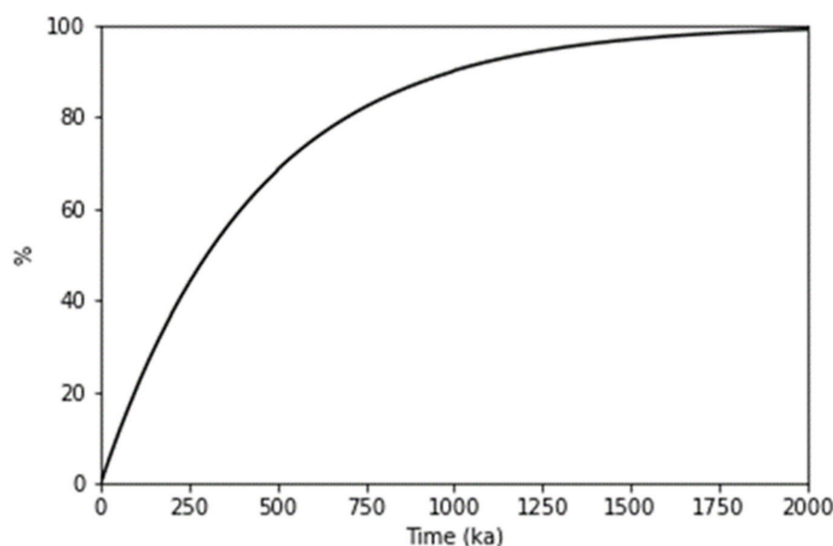


**Figure 2.** Modeled background production over time, shown as percent of the full equilibrium amount, based on Equation (1). Time to reach equilibrium is dependent on the half-life of  $^{36}\text{Cl}$ .

In this article, we present 89 cosmogenic  $^{36}\text{Cl}$  exposure ages, sampled from both glacial and volcanic landforms, all adjusted for the young rock formation ages. In addition, we present the results of the geochemical analyses for each sample, thereby adding to the previously available geochemical data from Jan Mayen [11].

A subset of the Jan Mayen samples provides evidence that the equilibrium assumption for background production should not be universally applied, with two samples even yielding measured  $^{36}\text{Cl}$  concentrations smaller than the calculated equilibrium background production. This provides an opportunity to investigate the influence of young bedrock formation ages on young exposure ages in the application of  $^{36}\text{Cl}$ .

### Study Area

Jan Mayen is situated on the Jan Mayen fracture zone in the North Atlantic ( $70^{\circ}5'–72^{\circ}\text{N}$ ;  $7^{\circ}5'–8^{\circ}5'\text{W}$ ; Figure 1). Nord-Jan, the northeast part of the small island, is dominated by the 2277 m high mountain Beerenberg, an active stratovolcano. The slopes of the volcano are covered by glaciers, a few of which reach down to sea level. In front of these glaciers are moraine ridges and other glacial deposits, with the most prominent of these assumed to be from the Little Ice Age, LIA, based on morphology, (lack of) vegetation cover, and historical observations [12]. In contrast, the southwestern part of the island, Sør-Jan, has a rougher and more variable topography, with its highest peak, Rudolf toppen, extending to

769 m. Nord-Jan and Sør-Jan are connected by Midt-Jan, a narrow (2–3 km wide) strip of land extending southwest from Beerenberg (Figure 1).

The oldest K/Ar age from the bedrock on Jan Mayen gives an age of only  $564 \pm 6$  ka [13], whereas the youngest bedrock on the island was formed during an eruption in 1985 [10,14]. Three other eruptions were observed in 1732, 1818, and 1970 [15,16], and it is likely that there were also at least two other eruptions in the 1650–1882 period [17].

The bedrock is dominated by trachybasaltic and ankaramitic lava flows [11,16,18], which have been grouped into three separate formations. The oldest of these, Havhestberget Formation, has limited surface exposure as it is mostly covered by the younger Nordvestkapp and Inndalen Formations. Of the two latter formations, the Nordvestkapp Formation predates the Last Glacial Maximum glaciation on Jan Mayen, and thus frequently shows signs of glacial reshaping, whereas the Inndalen Formation is largely of Holocene age and postdates the deglaciation of south and central Jan Mayen.

During the Last Glacial Maximum, all of Jan Mayen was covered by an ice cap, which most likely also reached out onto the surrounding continental shelf (Lyså et al. (2021) [1], partially based on a subset of the ages presented here).

## 2. Materials and Methods

### 2.1. Sampling Strategy

In total, 89 samples were collected for  $^{36}\text{Cl}$  dating on Jan Mayen between 2014 and 2018. The sampling focus of the early campaigns was on glacial landforms (e.g., boulders on moraine ridges, erratic boulders on till surfaces, and glacially abraded bedrock surfaces), but in the later campaigns, the young lava flows were also targeted (Figure 3).

The sample locations were recorded using a handheld GPS. All samples were preferentially collected from large, flat surfaces (dip  $<20^\circ$  for all samples). The samples were retrieved using hammer and a chisel (2014) and an electrical rock saw (2015–2018; Figure 3D). In addition to being much more efficient, we found that the use of an electrical rock saw resulted in thinner and more consistent sample thicknesses than what was achieved with only a hammer and chisel.

The topographic shielding at each sampling location was measured with a clinometer and compass. Topographic shielding was calculated from these measurements using the CRONUS Topographic Shielding Calculator v2.1. To enable topographic shielding measurements, sampling for cosmogenic surface exposure dating was preferentially performed on fair weather days, but the difficult logistics and maritime climate, which caused plenty of fog, meant that full visibility was not always possible (Figure 3C). In particular, the peak of Beerenberg was often hidden. Missing observations were replaced by the nearest measurements of the horizon angle or, when in the direction of Beerenberg, by our best estimate of the angle towards the peak. The sample elevations were measured by GPS and/or retrieved from the available small-scale map by the Norwegian Polar Institute (40 m contour interval).



**Figure 3.** Photographs showing selected sample locations. (A) JM2015-11, erratic boulder on till, Midt-Jan. (B) JM2018-74, lava, tindar on Sør-Jan. (C) JM2015-08, striated erratic boulder on till, Nord-Jan. (D) JM2015-01, erratic boulder on Nord-Jan. A battery-powered rock saw was used for sampling. (E) JM2018-113, lava flow. (F) Thin layer with plant material overlying a lava flow.

## 2.2. Sample Treatment and Measurements

Due to the fine-grained nature of the sampled volcanic rocks, they were processed as whole rock samples. The samples were prepared at the University of Bern Surface Exposure Dating Laboratory, based on the isotope dilution technique [19–21] and following the protocols by Stone et al. [22] and Ivy-Ochs et al. [20,23]. Before chemical treatment, the samples were crushed and sieved to a grain size of 250–400  $\mu\text{m}$  at the Geological Survey of Norway. Afterwards, the crushed material was leached twice to remove any possible non-in situ Cl contamination (e.g., Zreda et al. (1991) [24]). During leaching, 75 mL of 2M  $\text{HNO}_3$  and 500 mL ultrapure water were added to the samples, which were then left overnight before being successively rinsed four times with ultrapure water and dried on a hotplate at 60  $^\circ\text{C}$ . A  $\sim 10$  g aliquot was split from every sample for geochemical analysis, which was performed by Actlabs Analytical Services, Ontario, Canada. The major elements and relevant trace elements were measured using ICP and ICP-MS to enable the calculation of sample production rate (Table S1). A further 30 g of leached material was



processed in preparation for accelerator mass spectrometry (AMS) analysis. One chemical blank was processed along with batches of maximum 15 samples in order to determine the chemical background to be subtracted from the samples. Samples were spiked with roughly 2.5–3.5 mg of pure  $^{35}\text{Cl}$  carrier (99.63 atom %) in order to calculate the total Cl concentration ( $^{35}\text{Cl}$ ,  $^{37}\text{Cl}$ ) [20,23], and were then gradually dissolved with 30 mL of 14 M  $\text{HNO}_3$  and 120 mL of 40% HF. To remove the impurities and recover supernatant, the samples were centrifuged. Afterwards, 10 mL of 0.4 M  $\text{AgNO}_3$  solution was added in the dark to precipitate AgCl. The precipitated AgCl was collected and dissolved with 2 mL of  $\text{NH}_4\text{OH}$  (16% solution). In order to suppress the unwanted isobar of  $^{36}\text{S}$  from  $^{36}\text{Cl}$  through AMS measurements,  $\text{BaSO}_4$  precipitation was performed by adding  $\text{Ba}(\text{NO}_3)_2$ . At the final stage, AgCl was recovered in the form of a solid pill, rinsed with ultrapure water, and then dried. The AgCl pills were finally pressed into tantalum-lined copper targets for subsequent AMS measurements.

Concentrations of total Cl and  $^{36}\text{Cl}$  were measured by a single target at the ETH 6 MV Tandem AMS facility using a gas-filled magnet in combination with a gas-ionization chamber for separation of  $^{36}\text{Cl}$  from the isobar  $^{36}\text{S}$ , in accordance with the isotope dilution technique [20,25–27]. The stable ratio of  $^{37}\text{Cl}/^{35}\text{Cl}$  was normalized to the neutral ratio  $^{37}\text{Cl}/^{35}\text{Cl} = 31.98\%$  of the K382/4N standard and the machine blank. ETH internal standard K382/4N with a value of  $^{36}\text{Cl}/\text{Cl} = (17.36 \pm 0.35) \times 10^{-12}$  [26] was applied to normalize yielded ratios of  $^{36}\text{Cl}/^{35}\text{Cl}$ . The sulfur correction of the measured  $^{36}\text{Cl}/^{35}\text{Cl}$  ratio was not substantial. Moreover, measured  $^{36}\text{Cl}/^{35}\text{Cl}$  ratios of the sample were corrected for a procedural blank of  $(1 \pm 0.02) \times 10^{-15}$ . AMS results for blanks and carrier are included in Supplementary Table S3.

### 2.3. Calculations

Although initial exposure ages were calculated using the CRONUScalc web interface v. 2.0 [5], the model was not accurate for young samples on young volcanic material due to the built-in equilibrium assumption about background production. The CRONUScalc code was therefore modified directly in MATLAB to enable a flexible entry style allowing for calculation of three scenarios: (1) the rock formation age is sufficiently old that the equilibrium assumption for background production is reasonable (equivalent to CRONUScalc 2.1); (2) the rock formation age is known from independent constraints so the model implements Equation 1; and (3) the formation age of the rock is equal to the exposure age of the sample, so the exposure/formation age is solved iteratively. The inclusion of rock formation age as a required input is similar to the method used in the calculation spreadsheet in Schimmelpfennig et al. (2009) [7], but the calculations in CRONUScalc are fully automated rather than manual iteration on a sample-by-sample basis, and CRONUScalc allows easy access to time-dependent production rate scaling models. All CRONUScalc code, including these modifications, is publicly available on Bitbucket at <https://bitbucket.org/cronusearth/cronus-calc/> [accessed on 14 September 2021; v2.2, tag: Anjar\_et\_al\_2021\_JanMayen]. The CRONUScalc code was also updated and recalibrated to use the recently published rates for cosmogenic  $^{36}\text{Cl}$  production from iron published in Moore et al. (2019) [28]. These new rates are based on modern, robust analyses of multiple high-iron samples and can be incorporated in a similar format to the other spallation production rates already present in the code, unlike the previous Stone et al. (2005) rates [29]. This recalibration builds on the updated rates presented in Marrero et al. (2021) [30] and is discussed in more detail in Leontaritis (2021) [31]. Production rates of  $^{36}\text{Cl}$  from iron were derived for each scaling model by A. Moore [32], and these were fixed values in the recalibrations. The other production parameters were then recalibrated following the full procedure outlined in Marrero et al. (2016b) [9]. The new production rates are very similar to earlier rates and are given in Table 1. Iron oxide concentrations are >13 wt % in some samples, meaning that approximately 1–4% of production in the Jan Mayen samples is from this pathway. This has the potential to make a small but measurable difference in sample ages compared to results from CRONUScalc v2.1.



**Table 1.**  $^{36}\text{Cl}$  production rates for LM scaling model used to calculate these exposure ages. Percent change from Marrero et al. (2021) [30] (CRONUScal v2.1) is shown for comparison. See Marrero et al. (2016b) [9] for definitions of pathways. Muon parameter changes were all  $<0.07\%$ .

Pathway	Production Rate (at $^{36}\text{Cl}$ $\text{g}^{-1} \text{y}^{-1}$ )	% Change From v2.1
Ca—Spallation	$51.686 \pm 3.3$	−0.0003
K—Spallation	$150.996 \pm 10$	0.66
$P_f(0)$	$647.705 \pm 231$	0.37

Final results for exposure ages presented in this paper use the geomagnetically corrected Lal (1991) [33]/Stone (2000) [34] scaling (LM) [5,9] and  $^{36}\text{Cl}$  production rates from Marrero et al. (2021) [30] and Moore et al. (2019) [28], as described above. A range of rock formation ages ranging from infinite (yielding youngest exposure age) to “equal to exposure age” (yielding oldest possible exposure age) was used to evaluate a range of scenarios. Where nothing else is stated, the ages were calculated assuming a density of  $2.1 \pm 0.5 \text{ g/cm}^3$ , based on average density of Icelandic lava measured by Licciardi et al. (2008) [35], and assuming an erosion rate of  $1 \pm 0.5 \text{ mm/ky}$ . The input data used is presented in Supplementary Table S2.

#### 2.4. Radiocarbon Dating

One of the exposure-dated lava flows had been partially buried by sediments (in a different part than where the exposure samples were taken), and a pit was dug through the sediments and down into the lava flow. Unidentified plant material found directly overlying the lava flow (Figure 3F) was sampled for radiocarbon dating and dated at the National Laboratory for Age Determination, Trondheim, Norway. It was calibrated using OxCal v. 4.4 and the IntCal20 atmospheric curve [36].

### 3. Results and Interpretations

#### 3.1. Geochemistry

As part of the dating process, major elements and relevant trace elements were measured for all 89 samples (Supplementary Table S1) and the rock types were identified based on the geochemistry, following the classification in Le Maitre et al. (2002) [37]. A total of 18% of the samples were identified as Mg-rich rock types, mostly picrites, whereas the remaining samples were dominated by basalt, trachybasalt, and basaltic trachyandesite (Figure 4).

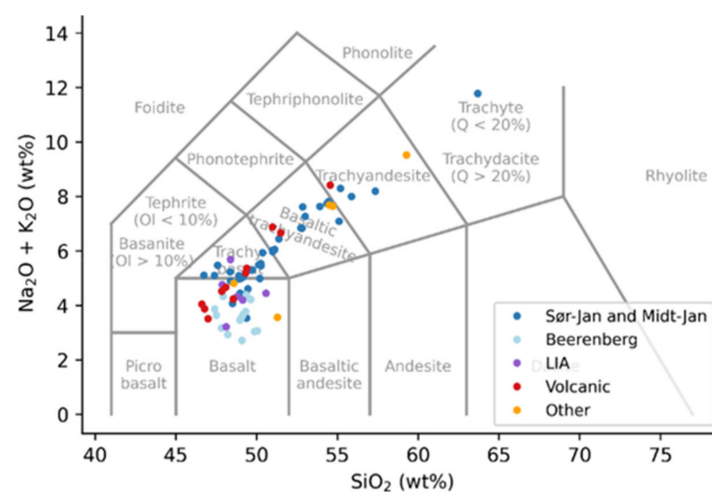


**Figure 4.** Rock-type classification based on the geochemistry of the samples. High-Mg ( $n = 15$ ) samples have been excluded as those are not classified with a TAS-plot. Additionally, samples JM2014-01 and JM2014-02 have been excluded due to methodological problems with their geochemistry measurements (see Supplementary Table S1). The colors are the same as in Figure 1.

### 3.2. Radiocarbon Date

The single radiocarbon sample was dated to 2.761–2.747 cal. ka BP (sample id: JM2019-122; Lab. id: Tra-14525;  $^{14}\text{C}$  age:  $2.643 \pm 0.017$   $^{14}\text{C}$  ka BP; calibrated age given with 1 sigma uncertainty). As the organic material was found directly overlying the lava flow, the radiocarbon age represents a minimum limiting age for both the lava flow and the two samples collected from the lava flow, JM2017-69 and JM2017-70.

### 3.3. Cosmogenic Nuclide Surface Exposure Age Dating

Samples were divided into three main groups: “glacial” samples, taken in settings where the exposure age is expected to reflect deglaciation; “volcanic” samples, e.g., from lava flows; and “other” samples, taken in settings where the exposure age is not directly related to the deglaciation or to volcanic activity (Figure 5). The glacial samples include samples taken from erratic boulders and striated bedrock. They were further subdivided into regions, with the lower lying areas in southern and central Jan Mayen (Sør-Jan and Midt-Jan, including some low-lying areas just north of Lake Nordlaguna) in one group ( $n = 41$ ), the slopes of Beerenberg in the second subgroup ( $n = 24$ ), and the samples taken from the fresh moraine ridges interpreted to be from the Little Ice Age in the third group ( $n = 8$ ). The volcanic samples ( $n = 11$ ) include samples from lava flows and from a tindar. The “other” samples ( $n = 5$ ) include a volcanic boulder deposited by a rock fall and two samples from a fluvially eroded setting.

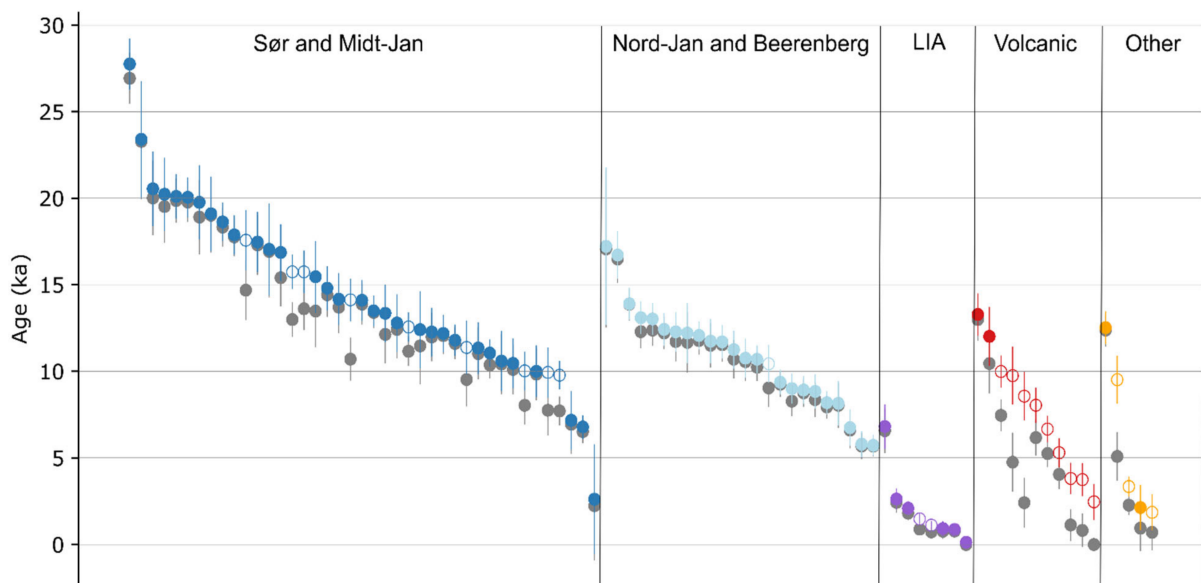


**Figure 5.** Exposure ages calculated assuming that the rock formation age equals the exposure age (i.e., young rock ages) in color, and below (in grey) the ages of the same sample calculated with the assumption that the background  $^{36}\text{Cl}$  had reached equilibrium. The samples have been separated into sample setting and region and sorted from the oldest to the youngest within each region. The uncertainties are the internal uncertainties (1 standard deviation). Samples where the equil. age differs by less than 1 standard deviation from the young rock age are indicated by filled circles, and if they differ by more than 1 standard deviation, indicated by unfilled circles.

Due to the young bedrock on Jan Mayen, we suspected that the background production might not have reached equilibrium, and all ages were therefore calculated with five different background production scenarios: (1) equilibrium assumption (equivalent to CRONUScalc 2.1), (2) rock formation at 564 ka (oldest dated rock on Jan Mayen [13]), (3) rock formation at 250 ka, (4) rock formation at 50 ka (250–50 ka represents the range of rock formation ages for the likely source formation for the glacial material), and (5) rock formation age equal to the exposure age of the sample (youngest possible rock formation age) (Table 2).

**Table 2.** Exposure ages calculated using five different scenarios for the background production. Our best estimate ages are indicated in bold. Calculated using LM scaling and assuming a density of  $2.1 \pm 0.5 \text{ g/cm}^3$  and an erosion rate of  $1 \pm 0.5 \text{ mm/ky}$ . See Supplementary Table S2 for the full set of sample information used in the calculations.

Name	Latitude WGS84	Longitude WGS84	Elevation	Equilibrium Assumption * (Equil.)			Formation Age = 564 ka			Formation Age = 250 ka			Formation Age = 50 ka			Formation Age = Exposure Age (Young Rock)		
				Age [ka]	Unc (ext)	Unc (int)	Age [ka]	Unc (ext)	Unc (int)	Age [ka]	Unc (ext)	Unc (int)	Age [ka]	Unc (ext)	Unc (int)	Age [ka]	Unc (ext)	Unc (int)
<i>Glacial samples—Sor Jan and Midt Jan</i>																		
JM2014-01	70.9751	−8.6210	114	19.8	1.6	1.2	19.9	1.6	1.2	19.9	1.6	1.2	<b>20.0</b>	1.6	1.2	20.0	1.6	1.2
JM2014-18	71.0144	−8.4514	52	7.7	1.6	0.8	8.3	1.6	0.8	8.9	1.7	0.8	<b>9.6</b>	1.8	0.8	9.8	1.9	0.8
JM2014-19	71.0104	−8.4334	119	13.4	1.1	0.9	13.4	1.1	0.9	13.4	1.1	0.9	<b>13.5</b>	1.1	0.9	13.5	1.1	0.9
JM2014-20	71.0123	−8.4226	144	11.6	1.2	0.9	11.7	1.2	0.9	11.7	1.2	0.9	<b>11.8</b>	1.2	0.9	11.8	1.2	0.9
JM2014-21	71.0129	−8.4121	162	19.0	2.4	2.2	19.0	2.4	2.2	19.1	2.4	2.2	<b>19.1</b>	2.4	2.2	19.1	2.4	2.2
JM2014-22	71.0227	−8.4404	55	11.2	1.2	0.8	11.5	1.3	0.8	12.0	1.3	0.9	<b>12.4</b>	1.3	0.9	12.6	1.3	0.8
JM2014-23	70.9896	−8.4967	71	19.9	1.6	1.3	19.9	1.6	1.3	20.0	1.6	1.3	<b>20.1</b>	1.6	1.3	20.1	1.6	1.3
JM2015-11	71.0193	−8.4489	41	10.4	1.8	1.7	10.5	1.8	1.7	10.5	1.8	1.7	<b>10.6</b>	1.8	1.7	10.6	1.8	1.7
JM2015-73	70.8673	−8.8091	45	7.7	1.6	1.5	8.4	1.6	1.5	9.0	1.6	1.5	<b>9.7</b>	1.7	1.5	9.9	1.7	1.4
JM2015-74	70.8680	−8.8063	32	10.7	1.7	1.2	11.7	1.8	1.2	12.7	1.9	1.2	<b>13.9</b>	2.0	1.2	14.1	2.0	1.2
JM2015-99	70.9707	−8.6012	115	10.1	1.5	1.4	10.2	1.5	1.4	10.3	1.5	1.4	<b>10.4</b>	1.5	1.4	10.5	1.5	1.4
JM2015-100	70.9734	−8.6085	109	2.2	3.2	3.2	2.3	3.2	3.2	2.5	3.2	3.2	<b>2.6</b>	3.2	3.2	2.6	3.2	3.2
JM2015-101	70.9732	−8.6095	100	12.4	1.8	1.7	12.5	1.8	1.7	12.6	1.8	1.7	<b>12.8</b>	1.8	1.7	12.8	1.8	1.7
JM2016-22	70.8974	−8.9312	310	20.0	2.6	2.2	20.2	2.6	2.2	20.3	2.6	2.2	<b>20.5</b>	2.6	2.2	20.5	2.6	2.2
JM2016-23	70.8924	−8.9137	412	17.3	1.9	1.7	17.3	1.9	1.7	17.4	1.9	1.7	<b>17.5</b>	1.9	1.7	17.5	1.9	1.7
JM2016-24	70.8894	−8.9146	437	13.5	3.0	2.1	14.0	3.1	2.1	14.6	3.1	2.1	<b>15.3</b>	3.2	2.1	15.5	3.2	2.1
JM2016-25	70.8924	−8.9304	258	19.5	2.6	2.1	19.7	2.7	2.1	19.9	2.7	2.1	<b>20.2</b>	2.7	2.1	20.2	2.7	2.1
JM2016-26	70.8923	−8.9300	258	18.9	2.8	2.1	19.1	2.8	2.1	19.4	2.9	2.1	<b>19.7</b>	2.9	2.1	19.8	2.9	2.1
JM2016-29	70.9281	−8.7716	393	12.1	2.1	1.7	12.5	2.2	1.7	12.8	2.2	1.7	<b>13.2</b>	2.2	1.7	13.3	2.2	1.7
JM2016-30	70.9294	−8.7822	366	12.0	1.5	1.4	12.1	1.5	1.4	12.1	1.5	1.4	<b>12.2</b>	1.5	1.4	12.3	1.5	1.4
JM2016-31	70.9581	−8.6804	265	14.4	1.5	1.3	14.5	1.5	1.3	14.6	1.5	1.3	<b>14.8</b>	1.5	1.3	14.8	1.5	1.3
JM2016-32	70.9501	−8.7037	337	14.7	3.1	1.7	15.5	3.2	1.7	16.4	3.4	1.7	<b>17.4</b>	3.5	1.7	17.6	3.5	1.7
JM2016-33	70.9513	−8.7423	202	13.7	1.7	1.5	13.8	1.7	1.5	14.0	1.7	1.5	<b>14.1</b>	1.7	1.5	14.2	1.7	1.5
JM2016-34	70.9519	−8.7368	217	11.5	2.4	2.2	11.7	2.4	2.2	12.0	2.5	2.2	<b>12.3</b>	2.5	2.2	12.4	2.5	2.2
JM2016-35	70.9508	−8.6906	318	13.9	1.4	1.2	13.9	1.4	1.2	14.0	1.4	1.2	<b>14.1</b>	1.4	1.2	14.1	1.4	1.2
JM2016-39	70.8699	−8.8181	126	9.5	1.7	1.6	10.0	1.8	1.6	10.6	1.8	1.6	<b>11.2</b>	1.8	1.6	11.4	1.8	1.6
JM2016-40	70.9300	−8.8159	205	11.0	1.6	1.5	11.1	1.6	1.5	11.2	1.6	1.5	<b>11.3</b>	1.6	1.5	11.3	1.6	1.5
JM2016-42	70.8776	−8.9529	321	23.3	3.5	3.3	23.3	3.5	3.3	23.4	3.5	3.3	<b>23.4</b>	3.5	3.3	23.4	3.5	3.3
JM2017-34	70.8474	−9.0162	180	18.3	1.5	1.1	18.4	1.5	1.1	18.5	1.5	1.1	<b>18.6</b>	1.5	1.1	18.6	1.5	1.1
JM2017-35	70.8410	−9.0084	211	10.4	1.0	0.8	10.6	1.0	0.8	10.8	1.0	0.8	<b>11.0</b>	1.0	0.8	11.0	1.0	0.8
JM2017-36	70.8413	−8.9938	231	16.9	2.8	2.7	17.0	2.8	2.7	17.0	2.8	2.7	<b>17.0</b>	2.8	2.7	17.0	2.8	2.7
JM2017-42	71.0011	−8.4445	320	17.8	1.4	1.1	17.8	1.4	1.1	17.8	1.4	1.1	<b>17.9</b>	1.4	1.1	17.9	1.4	1.1
JM2017-45	70.8955	−8.8458	605	6.5	0.8	0.7	6.6	0.8	0.7	6.7	0.8	0.7	<b>6.8</b>	0.8	0.7	6.8	0.8	0.7
JM2017-56	71.0041	−8.4871	51	12.1	1.2	1.1	12.1	1.2	1.1	12.1	1.2	1.1	<b>12.2</b>	1.2	1.1	12.2	1.2	1.1
JM2017-57	71.0041	−8.4871	51	9.8	1.6	1.5	9.9	1.6	1.5	9.9	1.6	1.5	<b>10.0</b>	1.6	1.5	10.0	1.6	1.5
JM2017-58	71.0091	−8.3948	230	15.4	2.0	1.6	15.8	2.1	1.6	16.3	2.1	1.6	<b>16.8</b>	2.1	1.6	16.9	2.1	1.6

Table 2. Cont.

Name	Latitude WGS84	Longitude WGS84	Elevation	Equilibrium Assumption * (Equil.)			Formation Age = 564 ka			Formation Age = 250 ka			Formation Age = 50 ka			Formation Age = Exposure Age (Young Rock)		
				Age [ka]	Unc (ext)	Unc (int)	Age [ka]	Unc (ext)	Unc (int)	Age [ka]	Unc (ext)	Unc (int)	Age [ka]	Unc (ext)	Unc (int)	Age [ka]	Unc (ext)	Unc (int)
	[dd]	[dd]	[m]															
JM2017-59	71.0133	−8.3844	334	26.9	2.3	1.5	27.2	2.4	1.5	27.4	2.4	1.5	27.7	2.4	1.5	27.8	2.4	1.5
JM2017-64	70.9941	−8.4626	29	13.0	1.5	1.0	13.8	1.6	1.0	14.6	1.6	1.0	15.5	1.7	1.0	15.7	1.7	1.0
JM2017-65	71.0129	−8.4459	71	6.9	1.7	1.7	7.0	1.7	1.7	7.1	1.7	1.7	7.1	1.7	1.7	7.2	1.7	1.7
JM2017-66	71.0146	−8.4501	41	13.6	2.7	1.2	14.2	2.8	1.2	14.9	2.9	1.2	15.6	3.1	1.2	15.7	3.1	1.2
JM2017-67	71.0148	−8.4506	41	8.0	1.7	1.1	8.6	1.8	1.1	9.2	1.9	1.1	9.8	2.0	1.1	10.0	2.0	1.1
<i>Glacial samples–Beerenberg</i>																		
JM2014-02	70.9955	−8.2571	116	13.9	1.3	0.9	13.9	1.3	0.9	13.9	1.3	0.9	13.9	1.3	0.9	13.9	1.3	0.9
JM2014-03	70.9971	−8.2528	140	11.8	1.4	0.8	11.9	1.4	0.8	11.9	1.4	0.8	12.0	1.4	0.8	12.1	1.4	0.8
JM2014-04	70.9976	−8.2515	144	10.2	1.8	0.8	10.4	1.8	0.8	10.5	1.8	0.8	10.7	1.8	0.8	10.7	1.8	0.8
JM2014-05	71.0021	−8.2298	170	8.8	0.9	0.8	8.8	0.9	0.8	8.8	0.9	0.8	8.9	0.9	0.8	8.9	0.9	0.8
JM2014-10	71.0008	−8.1782	156	5.7	0.8	0.8	5.7	0.8	0.8	5.7	0.8	0.8	5.8	0.8	0.8	5.8	0.8	0.8
JM2014-11	71.0003	−8.1790	153	6.6	1.1	1.1	6.6	1.1	1.1	6.7	1.1	1.1	6.7	1.1	1.1	6.7	1.1	1.1
JM2014-12	70.9962	−8.1883	81	9.3	0.9	0.7	9.3	0.9	0.7	9.3	0.9	0.7	9.4	0.9	0.7	9.4	0.9	0.7
JM2014-13	71.0040	−8.1531	223	8.3	1.7	0.9	8.5	1.7	0.9	8.7	1.7	0.9	8.9	1.8	0.9	9.0	1.8	0.9
JM2014-14	71.0043	−8.1532	233	12.4	2.1	0.9	12.6	2.1	0.9	12.8	2.1	0.9	13.0	2.1	0.9	13.0	2.2	0.9
JM2014-15	71.0040	−8.1331	179	16.5	1.6	1.4	16.5	1.6	1.4	16.6	1.6	1.4	16.7	1.6	1.4	16.7	1.6	1.4
JM2014-16	71.0041	−8.1333	181	7.9	0.8	0.7	8.0	0.8	0.7	8.1	0.8	0.7	8.2	0.8	0.7	8.2	0.8	0.7
JM2014-17	70.9976	−8.1844	47	10.6	1.2	1.1	10.6	1.2	1.1	10.7	1.2	1.1	10.7	1.2	1.1	10.8	1.2	1.1
JM2015-01	71.0291	−8.3451	460	12.3	1.9	0.9	12.5	1.9	0.9	12.8	1.9	0.9	13.0	2.0	0.9	13.1	2.0	0.9
JM2015-02	71.0291	−8.3451	460	8.0	1.4	1.3	8.1	1.4	1.3	8.1	1.4	1.3	8.1	1.4	1.3	8.2	1.4	1.3
JM2015-03	71.0307	−8.3239	552	5.7	0.7	0.6	5.7	0.7	0.6	5.7	0.7	0.6	5.7	0.7	0.6	5.7	0.7	0.6
JM2015-07	71.0530	−8.4027	122	8.4	1.2	1.0	8.5	1.2	1.0	8.6	1.2	1.0	8.8	1.2	1.0	8.8	1.2	1.0
JM2015-08	71.0519	−8.3994	122	11.7	2.0	1.7	11.8	2.0	1.7	12.0	2.0	1.7	12.2	2.1	1.7	12.2	2.1	1.7
JM2015-33	71.0032	−8.1487	213	9.0	2.0	1.1	9.4	2.1	1.1	9.8	2.1	1.1	10.3	2.2	1.1	10.4	2.2	1.1
JM2015-34	71.0046	−8.1360	195	11.5	1.5	1.3	11.6	1.5	1.3	11.6	1.5	1.3	11.7	1.5	1.3	11.7	1.5	1.3
JM2015-42	71.0517	−8.3676	306	10.7	1.5	1.1	10.8	1.5	1.1	11.0	1.5	1.1	11.2	1.6	1.1	11.2	1.6	1.1
JM2017-14	70.9983	−8.2588	145	11.5	1.3	1.0	11.6	1.3	1.0	11.6	1.3	1.0	11.7	1.3	1.0	11.7	1.3	1.0
JM2017-15	71.0161	−8.2402	367	12.2	1.2	0.9	12.3	1.2	0.9	12.3	1.2	0.9	12.4	1.2	0.9	12.4	1.2	0.9
JM2017-18	71.0043	−8.1198	84	17.1	4.6	4.6	17.1	4.6	4.6	17.2	4.6	4.6	17.2	4.6	4.6	17.2	4.6	4.6
JM2017-19	71.0026	−8.1165	67	11.7	1.4	1.1	11.9	1.5	1.1	12.0	1.5	1.1	12.2	1.5	1.1	12.3	1.5	1.1
<i>Glacial samples–Little Ice Age moraines</i>																		
JM2014-06	71.0035	−8.2217	191	6.6	1.4	1.3	6.6	1.4	1.3	6.7	1.4	1.3	6.8	1.4	1.3	6.8	1.4	1.3
JM2014-08	70.9992	−8.1929	162	0.8	0.4	0.4	0.8	0.4	0.4	0.9	0.4	0.4	0.9	0.4	0.4	0.9	0.4	0.4
JM2014-09	71.0003	−8.1905	191	0.0	0.0	0.0	0.0	0.0	0.0	0.0	0.4	0.4	0.1	0.4	0.4	0.1	0.4	0.4
JM2015-04	71.0314	−8.3225	565	0.9	0.3	0.3	1.0	0.3	0.3	1.2	0.3	0.3	1.4	0.3	0.3	1.5	0.3	0.3
JM2015-05	71.0341	−8.3190	602	2.4	0.6	0.6	2.5	0.6	0.6	2.5	0.6	0.6	2.6	0.6	0.6	2.6	0.6	0.6
JM2015-06	71.0336	−8.3171	604	0.8	0.3	0.3	0.8	0.3	0.3	0.8	0.3	0.3	0.9	0.3	0.3	0.9	0.3	0.3
JM2015-43	71.0564	−8.3367	491	0.7	0.2	0.2	0.8	0.2	0.2	0.9	0.2	0.2	1.1	0.2	0.2	1.1	0.2	0.2
JM2015-44	71.0576	−8.3424	462	1.8	0.4	0.4	1.9	0.4	0.4	2.0	0.4	0.4	2.1	0.4	0.4	2.1	0.4	0.4

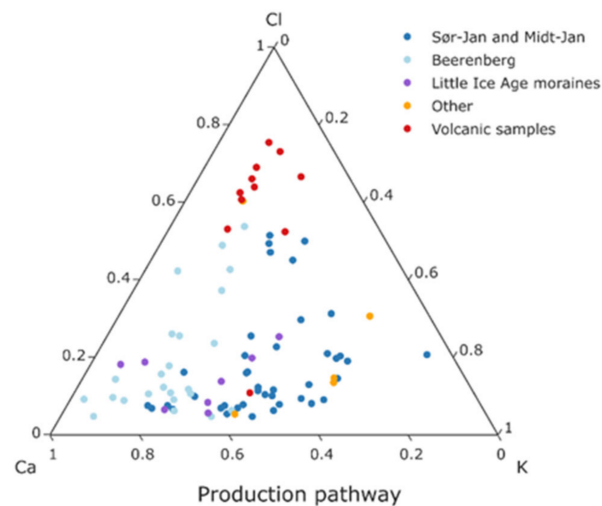


Table 2. Cont.

Name	Latitude WGS84	Longitude WGS84	Elevation	Equilibrium Assumption * (Equil.)			Formation Age = 564 ka			Formation Age = 250 ka			Formation Age = 50 ka			Formation Age = Exposure Age (Young Rock)		
				Age [ka]	Unc (ext)	Unc (int)	Age [ka]	Unc (ext)	Unc (int)	Age [ka]	Unc (ext)	Unc (int)	Age [ka]	Unc (ext)	Unc (int)	Age [ka]	Unc (ext)	Unc (int)
	[dd]	[dd]	[m]															
<i>Other samples</i>																		
JM2014-24	70.9145	−8.7853	428	2.3	0.7	0.6	2.6	0.8	0.6	2.9	0.8	0.6	<b>3.2</b>	0.9	0.6	3.3	0.9	0.6
JM2015-62	71.0043	−8.4476	63	5.1	1.5	1.4	6.3	1.6	1.4	7.6	1.6	1.4	<b>9.1</b>	1.7	1.4	9.5	1.8	1.4
JM2016-27	70.8772	−9.0040	26	0.7	1.0	1.0	1.0	1.0	1.0	1.4	1.0	1.0	<b>1.7</b>	1.0	1.0	1.9	1.0	1.0
JM2016-28	70.8772	−9.0040	42	0.9	1.3	1.3	1.3	1.3	1.3	1.6	1.3	1.3	<b>2.0</b>	1.3	1.3	2.1	1.3	1.3
JM2018-74	70.9633	−8.5863	165	12.4	1.1	1.0	12.4	1.1	1.0	12.5	1.1	1.0	<b>12.5</b>	1.1	1.0	12.5	1.1	1.0
<i>Volcanic samples</i>																		
JM2017-37	70.8591	−9.0499	2	4.8	2.1	1.7	6.2	2.3	1.7	7.6	2.5	1.7	9.3	2.9	1.7	<b>9.7</b>	2.9	1.7
JM2017-39	70.8785	−8.9971	21	2.4	1.5	1.4	4.1	1.7	1.4	6.0	2.0	1.4	8.0	2.3	1.4	<b>8.6</b>	2.4	1.4
JM2017-43	70.9018	−8.7814	181	7.5	1.6	0.9	8.2	1.7	0.9	8.9	1.9	0.9	9.8	2.0	0.9	<b>10.0</b>	2.0	0.9
JM2017-69	70.9251	−8.7082	18	1.1	1.0	0.9	1.9	1.0	0.9	2.7	1.1	0.9	3.5	1.2	0.9	<b>3.8</b>	1.2	0.9
JM2017-70	70.9244	−8.7145	26	0.8	1.0	1.0	1.6	1.0	1.0	2.5	1.1	1.0	3.5	1.2	1.0	<b>3.7</b>	1.3	1.0
JM2018-101	70.9170	−8.8396	290	6.2	1.8	1.0	6.7	1.9	1.0	7.2	2.0	1.0	7.9	2.1	1.0	<b>8.0</b>	2.2	1.0
JM2018-107	70.8969	−8.9121	285	13.0	1.4	1.2	13.1	1.4	1.2	13.2	1.4	1.2	13.3	1.4	1.2	<b>13.3</b>	1.4	1.2
JM2018-109	70.8835	−8.9459	250	5.3	1.4	0.8	5.6	1.4	0.8	6.1	1.5	0.8	6.5	1.6	0.8	<b>6.7</b>	1.6	0.8
JM2018-111	70.9175	−8.8796	70	10.4	2.8	1.7	10.9	2.8	1.7	11.4	2.9	1.7	11.9	3.0	1.7	<b>12.0</b>	3.0	1.7
JM2018-113	70.9131	−8.7384	60	4.0	1.1	0.8	4.4	1.2	0.8	4.8	1.2	0.8	5.2	1.3	0.8	<b>5.3</b>	1.3	0.8
JM2018-115	70.9092	−8.7533	150	0.0	0.0	0.0	0.0	0.0	0.0	0.8	1.1	1.1	2.1	1.2	1.1	<b>2.5</b>	1.2	1.0

\* Original using updated Fe

Proportions of cosmogenic  $^{36}\text{Cl}$  attributed to the three major production pathways (K, Ca, and Cl) varies substantially between the samples (Figure 6). Samples with a higher proportion of production from the Cl pathway are more likely to be affected by the formation age assumption. The range of possible scenarios surrounding the background production is discussed in detail later.



**Figure 6.** Ternary plot indicating the contributions from each major production pathway. The samples have been normalized so that the Ca production + K production + Cl production = 100%. The colors indicate sample region (the same colors as in Figure 1).

#### 4. Discussion

##### 4.1. Evaluation of General Uncertainties

The dominant reactions that produce cosmogenic  $^{36}\text{Cl}$  target K, Ca, and  $^{35}\text{Cl}$  in the rock (Figure 6). Whereas  $^{36}\text{Cl}$  production through spallation of K and Ca is reasonably well constrained, the production of  $^{36}\text{Cl}$  by  $^{35}\text{Cl}$  neutron capture is more complicated, and sensitive to, e.g., composition, water content, and snow cover [7–9,38]. This means that higher Cl concentrations lead to larger age uncertainties for those samples. Marrero et al. (2016) [9] defined a high Cl sample as a sample with more than 80 ppm Cl, which applies to 27 of our samples, with a maximum of 835 ppm in JM2018-115. Although all samples are taken from volcanic rocks, the samples collected to examine volcanic aspects have particularly high Cl contents compared with samples collected for other purposes (9 out of 11 volcanic samples are affected, Figure 5). The reason for this is unclear.

The erosion rate will affect the  $^{36}\text{Cl}$  exposure ages but is unmeasured on Jan Mayen. As an estimate, we therefore used an erosion rate of  $1 \pm 0.5$  mm/ky, similar to what has previously been used in Iceland (1.11 mm/ky [39]). Changing the estimated erosion rates to either  $0 \pm 0$  mm/ky or  $2 \pm 0.5$  mm/ky changes the calculated ages by, on average, less than 1%. If a substantially higher erosion rate is used, e.g., 5 mm/ky, there is an average change of ~2%, although for a small number of samples, the effect is more pronounced (5 samples changed 5–7%).

The sample density will also have a small influence on the calculated ages. Although sample densities were not measured in this study, we assume densities measured by Licciardi et al. (2008) [35] for lava flows in Iceland, ranging from 1.76 to 2.44 g/cm<sup>3</sup>, are likely to be similar to densities on Jan Mayen. We have therefore assumed a density of  $2.1 \pm 0.5$  g/cm<sup>3</sup> for all samples, but the typically variable vesicularity of the sampled volcanic rocks indicates that a substantial spread in the true density of the samples is likely. To test the sensitivity of the reported ages to erosion, we calculated the ages using densities of 1.7 and 2.5 g/cm<sup>3</sup>. The resulting ages changed by an average of <1%, well within uncertainties.

The production of cosmogenic nuclides can also be temporally influenced by local shielding effects, such as vegetation and snow or soil cover. The present-day vegetation on Jan Mayen is sparse (Figure 3) and not expected to influence the ages. Snow cover could be more important, but the maritime climate on Jan Mayen causes warm winters and generally thin snow cover, at least on lower elevations. Wind drift in the very open landscape could cause more substantial snow cover in shielded positions, but we consider the existing observations insufficient for estimating snow thickness for our samples and have, therefore, not corrected for snow shielding.

In addition, isostasy and topographic shielding will also influence the ages. The present-day topographic shielding was measured in the field, and although poor visibility limited the observations for some of the samples, we consider the actual influence of these uncertainties on the ages to be small, as most of the samples were taken in reasonably open terrain and during at least partial visibility. The possible exceptions are samples JM2017-36 and JM2018-101, for which no shielding measurements were possible. Isostatic changes will also have some influence on the calculated exposure ages as they may change the elevation of a sample. A recent study by Larsen et al. (2021) [2] identified a 14 m vertical tectonic displacement of southwest Beerenberg, following an eruption in 1732. So far, this is the only documented postglacial displacement, but we cannot exclude that there have been other instances of vertical displacements on the island due to both glacioisostasy and volcanic activity. As the extent and duration of such changes are difficult to quantify, no corrections are included here.

#### 4.2. Influence of Young Bedrock

A unique problem for  $^{36}\text{Cl}$  dating in a young volcanic landscape, such as Jan Mayen, is that the background production and decay have not necessarily reached equilibrium (Figure 2). The Jan Mayen samples provide additional evidence that the equilibrium assumption should not be applied to all samples. If equilibrium is (incorrectly) assumed for our samples, background production of  $^{36}\text{Cl}$  is calculated to contribute to between 0.2 and 196.5% of the total measured  $^{36}\text{Cl}$  in the samples. The latter value is clearly unreasonable, so we interpret it as an indication that these rocks have not reached equilibrium, which takes approximately 2 million years for  $^{36}\text{Cl}$ . This is in agreement with the independent ages indicating that the bedrock is generally young. To estimate the potential influence of rock formation age, we considered five different scenarios for the rock formation age: equilibrium conditions, rock formation at 564, 250, or 50 ka, and assuming that rock formation age equaled the exposure age. In the following discussion, “equil.” is used when referring to ages calculated assuming equilibrium conditions, and “young rock” is used to indicate ages calculated assuming that the exposure age equals the rock age.

Although all samples were calculated with multiple scenarios, the calculated age of most of the samples were relatively unaffected. However, as expected, there are a subset of samples that are more significantly affected by rock formation age assumptions (Figure 5). We observe, in detail, these samples to investigate these effects further. Specifically, we define “significantly affected” as samples where the compared ages differed by more than one standard deviation. For 25 samples, the age calculated assuming young rock conditions was more than one standard deviation from the age calculated using equilibrium conditions, with a maximum age difference of 6.1 ka in sample JM2017-39. Using a more realistic comparison between the oldest known rock formation age on Jan Mayen (564 ka) and the young rock scenario reduces the number of significantly affected samples to 22, with a maximum deviation of 4.4 ka.

The worst affected samples largely coincide with the samples classified as high Cl (>80 ppm, 19 out of 25 significantly affected samples), as would be expected since  $^{35}\text{Cl}$  is required for background production. Although U and Th concentrations are not especially high (<10 ppm in all cases), the high native Cl concentrations and short exposure durations are sufficient to illustrate the issue. Older samples are less significantly affected because

the potential difference between the equil. and nonequil. age becomes smaller through time due to the build-up of the background signal.

For volcanic samples such as lava flows, it is often reasonable to assume that the rock formation age is the same as the exposure age. The question is then whether or not the rock contains any  $^{36}\text{Cl}$  formed before the lava solidified. Schimmelpfennig et al. (2009) [7] found that the total  $^{36}\text{Cl}$  content in a fully shielded, high-Cl (1093 ppm), 400-year-old lava flow was close to the background values of  $^{36}\text{Cl}$  found in the blanks, suggesting minimal contributions of  $^{36}\text{Cl}$  formed before the lava solidified. Results from our only two samples collected from an independently-dated Jan Mayen lava flow support this. Samples JM2017-69 and JM2017-70 were dated to  $1.1 \pm 1$  ka and  $0.8 \pm 1$  ka when assuming equilibrium conditions, but to  $3.8 \pm 1.2$  ka and  $3.7 \pm 1.3$  ka when using the young rock age. Only the young rock age agrees with the minimum limiting age from radiocarbon dated plant material found directly overlying the same lava flow, which was dated to 2.761–2.747 cal. ka BP. Two additional samples, JM2014-09 and JM2018-115, had estimated equil. levels of background  $^{36}\text{Cl}$  well above the measured total  $^{36}\text{Cl}$  concentration (background + cosmogenic), indicating that those samples were not in equilibrium. We therefore conclude that the young rock age gives a better age estimate for the volcanic samples.

Even the oldest bedrock on the island ( $564 \pm 6$  ka [13]) has only reached a background production value of ~73% of the equilibrium value (Figure 2). For nonvolcanic samples, it is reasonable to assume that the rock formation age is unrelated to the exposure age, meaning that the true rock formation age lies somewhere between 564 ka and the young rock age. However, most of the glacial samples likely originate from the Nordvestkapp formation (Figure 1), which covers much of the land surface and which predates the deglaciation on south and central Jan Mayen. Most of the K/Ar and Ar/Ar dates from this formation fall between 50 and 250 ka [1,10,13]), which means that the background contribution has reached roughly 10–45% of the equilibrium values. We therefore suggest that the 50 ka and 250 ka formation age scenarios probably give the most accurate ages for these samples, and we use the 50 ka scenario as our best estimate for all the nonvolcanic samples. However, while this interpretation is reasonable on the group level, it does not necessarily hold true for a specific individual sample, and we therefore recommend that the 13 nonvolcanic samples with substantial (>1 standard deviation) difference between the 564 ka scenario age and the young rock age be interpreted with this potential variability in mind.

#### 4.3. Deglaciation Pattern

Although an in-depth discussion of the deglaciation on Jan Mayen is outside the scope of this paper, some general conclusions can be drawn from the cosmogenic exposure ages alone. Note that as we consider the assumption of rock formation at 50 ka to be the most appropriate scenario for glacial samples, it has been used throughout this section. Choice of bedrock formation age model only slightly affects the general deglaciation pattern discussed here, with older formation ages leading to slightly younger exposure ages (Figure 5). For a more extensive discussion on the deglaciation on Jan Mayen, see Lyså et al. (2021) [1].

On south and central Jan Mayen, ages taken from glacial settings range from 27.7 to 2.6 ka, with a median value of 13.9 ka ( $n = 41$ , Figure 5). All but two of the ages are ~20 ka or younger, suggesting that deglaciation in this part started properly around 20 ka (Figure 5). In addition, 38 out of the 41 samples give ages in the interval from 20.5 to 6.8 ka, suggesting that most of south and central Jan Mayen became ice free during this time period. Only the final glacial age from this area, JM2015-100, with an age of  $2.6 \pm 3.2$  ka, deviates from this general deglaciation pattern. On Nord-Jan and the slopes of Beerenberg, the deglaciation appears to begin somewhat later, as would be expected around a 2277 m high mountain, with deglaciation ages ranging from 17.2 to 5.7 ka (median 11.0 ka,  $n = 24$ ), and all but two of them younger than 14 ka (Figure 5).

Apart from a single outlier age at 2.6 ka, none of the glacial samples taken outside of the LIA moraines is younger than 5.7 ka, and it seems reasonable to assume that the



glaciers have been at or inside the LIA moraines for the last 5–6 thousand years. The eight samples from the LIA moraines range in age from 6.8 to 0.1 ka, with five of them giving ages younger than 1.5 ka (Figure 5).

## 5. Conclusions

- In this study, we present 89 cosmogenic exposure ages ( $^{36}\text{Cl}$ ) from Jan Mayen, most of them dating either the deglaciation ( $n = 73$ ) or postglacial volcanic events ( $n = 11$ ) on the island.
- Based on the range of exposure ages at each location, large-scale deglaciation on Jan Mayen began  $\sim 20$  ka and continued until 5.7 ka, after which the glaciers appear to have retreated inside the Little Ice Age moraines.
- The exposure ages on Jan Mayen were calculated using an updated version of CRONUScalc to account for the young bedrock formation ages at the site. Although the formation age assumption does not significantly affect most samples ( $n = 64$ ), a number of exposure ages change substantially ( $n = 25$ ) depending on the rock formation age assumed for the sample. On Jan Mayen, the most appropriate assumption for rock formation age varied by sample group: for samples dating volcanic activity, formation age should be assumed equal to the exposure age, whereas a rock formation age of 50 ka was used for the remaining samples.
- We recommend not assuming equilibrium conditions when calculating  $^{36}\text{Cl}$  ages on rocks that meet the following criteria: (i) known young rock formation ages, and (ii) potentially susceptible composition, specifically high native Cl, or high U and/or Th concentrations that are likely to occur in volcanic rocks. Young exposure age samples will be particularly affected because of the large mismatch between expected equilibrium conditions and measured concentrations.

**Supplementary Materials:** The following are available online at <https://www.mdpi.com/article/10.3390/geosciences11090390/s1>: Supplementary Spreadsheet that includes Supplementary Table S1: Sample geochemistry results; Supplementary Table S2: All sample inputs for CRONUScalc calculations; Table S3: AMS data for all samples.

**Author Contributions:** A.L. and E.A.L. did most of the fieldwork, N.M. did most of the sample preparations under N.A.'s guidance, whereas C.V. performed the  $^{36}\text{Cl}$  measurements. S.M. did most of the age calculations and adapted the CRONUScalc code for variable background production scenarios. J.A. participated in some of the fieldwork (2015), did some of the sample preparation and age calculations, and wrote most of the manuscript, with major contributions from S.M. and substantial contributions from the other coauthors. J.A., N.A., E.A.L., A.L., S.M., N.M. and C.V. all contributed to the interpretations and to the final version of the manuscript. Two anonymous reviewers gave constructive comments on the manuscript. All authors have read and agreed to the published version of the manuscript.

**Funding:** Financial support was given by the Geological Survey of Norway, The Research Council of Norway to A. Lyså (Grant No. 244135/E10 and Arctic Field Grant 2014), and to A. Lyså through The Royal Norwegian Society of Sciences and Letters (2019, DKNVS). Logistical support, and necessary permissions, were provided by the County Governor of Nordland and the Norwegian Defence Logistic Organisation (CYFOR, Jan Mayen).

**Data Availability Statement:** The complete geochemistry dataset and all the sample data used in the exposure age calculations are included in the supplementary material.

**Conflicts of Interest:** The authors declare no conflict of interest.

## References

1. Lyså, A.; Larsen, E.A.; Anjar, J.; Akçar, N.; Ganerød, M.; Hiksdaal, A.; Van Der Lelij, R.; Vockenhuber, C. The last glaciation of the Arctic volcanic island Jan Mayen. *Boreas* **2021**, *50*, 6–28. [[CrossRef](#)]
2. Larsen, E.; Lyså, A.; Höskuldsson, Á.; Davidsen, J.G.; Nadeau, M.J.; Power, M.; Tassis, G.; Wastegård, S. A dated volcano-tectonic deformation event in Jan Mayen causing landlocking of Arctic charr. *J. Quat. Sci.* **2021**, *36*, 180–190. [[CrossRef](#)]

3. Dallmann, W.K. Berggrunnsgeologi Jan Mayen. In *Natur og Kulturmiljøet på Jan Mayen—Med en Vurdering av Verneverdier, Kunnskapsbehov og Forvaltning*; Gabrielsen, G.W., Brekke, B., Alsos, I.G., Hansen, J.R., Eds.; Norsk Polarinstittutt Meddelelser: Tromso, Norway, 1997; Volume 144, p. 35.
4. Gosse, J.C.; Phillips, F.M. Terrestrial in situ cosmogenic nuclides: Theory and application. *Quat. Sci. Rev.* **2001**, *20*, 1475–1560. [[CrossRef](#)]
5. Marrero, S.M.; Phillips, F.M.; Borchers, B.; Lifton, N.; Aumer, R.; Balco, G. Cosmogenic nuclide systematics and the CRONUScal program. *Quat. Geochronol.* **2016**, *31*, 160–187. [[CrossRef](#)]
6. Phillips, F.M.; Plummer, M.A. Chloé: A Program for Interpreting in-Situ Cosmogenic Nuclide Data for Surface Exposure Dating and Erosion Studies. *Radiocarbon* **1996**, *38*, 98–99.
7. Schimmelpfennig, I.; Benedetti, L.; Finkel, R.; Pik, R.; Blard, P.-H.; Bourlès, D.; Burnard, P.; Williams, A. Sources of in-situ  $^{36}\text{Cl}$  in basaltic rocks. Implications for calibration of production rates. *Quat. Geochronol.* **2009**, *4*, 441–461. [[CrossRef](#)]
8. Parmelee, D.E.; Kyle, P.R.; Kurz, M.D.; Marrero, S.M.; Phillips, F.M. A new Holocene eruptive history of Erebus volcano, Antarctica using cosmogenic  $^3\text{He}$  and  $^{36}\text{Cl}$  exposure ages. *Quat. Geochronol.* **2015**, *30*, 114–131. [[CrossRef](#)]
9. Marrero, S.; Phillips, F.M.; Caffee, M.W.; Gosse, J.C. CRONUS-Earth cosmogenic  $^{36}\text{Cl}$  calibration. *Quat. Geochronol.* **2016**, *31*, 199–219. [[CrossRef](#)]
10. Cromwell, G.; Tauxe, L.; Staudigel, H.; Constable, C.G.; Koppers, A.A.P.; Pedersen, R.-B. In search of long-term hemispheric asymmetry in the geomagnetic field: Results from high northern latitudes (Dataset). *Geochem. Geophys. Geosyst.* **2013**, *14*, 3234–3249. [[CrossRef](#)]
11. White, C.A. Petrology and Mineral Chemistry of Some Jan Mayen Volcanics. Master’s Thesis, State University of New York at Albany, Albany, NY, USA, 1979.
12. Anda, E.O.O.; Mangerud, J.A.N. Late Holocene Glacier Variations and Climate at Jan Mayen. *Polar Res.* **1985**, *3*, 129–140. [[CrossRef](#)]
13. Larsen, E. (Geological Survey of Norway, Trondheim, Norway). Personal communication, 2021.
14. Imsland, P. The Volcanic Eruption on Jan Mayen, January 1985: Interaction between a Volcanic Island and a Fracture Zone. *J. Volcanol. Geotherm. Res.* **1986**, *28*, 45–53. [[CrossRef](#)]
15. Gjelsvik, T. Volcano on Jan Mayen Alive Again. *Nat. Cell Biol.* **1970**, *228*, 352. [[CrossRef](#)]
16. Sylvester, A.G. History and surveillance of volcanic activity on Jan Mayen island. *Bull. Volcanol.* **1975**, *39*, 313–335. [[CrossRef](#)]
17. Gjerløw, E. Holocene Volcanic Activity and Hazards of Jan Mayen, North-Atlantic. Ph.D. Thesis, University of Bergen, Bergen, Norway, 2018.
18. Maaloe, S.; Sorensen, I.; Hertogen, J. The Trachybasaltic Suite of Jan Mayen. *J. Pet.* **1986**, *27*, 439–466. [[CrossRef](#)]
19. Elmore, D.; Ma, X.; Miller, T.; Mueller, K.; Perry, M.; Rickey, F.; Sharma, P.; Simms, P.; Lipschütz, M.; Vogt, S. Status and plans for the PRIME Lab AMS facility. *Nucl. Instrum. Methods Phys. Res. Sect. B Beam Interact. Mater. Atoms* **1997**, *123*, 69–72. [[CrossRef](#)]
20. Ivy-Ochs, S.; Synal, H.-A.; Roth, C.; Schaller, M. Initial results from isotope dilution for Cl and  $^{36}\text{Cl}$  measurements at the PSI/ETH Zurich AMS facility. *Nucl. Instrum. Methods Phys. Res. Sect. B Beam Interact. Mater. Atoms* **2004**, *223–224*, 623–627. [[CrossRef](#)]
21. Desilets, D.; Zreda, M.; Almasi, P.F.; Elmore, D. Determination of cosmogenic  $^{36}\text{Cl}$  in rocks by isotope dilution: Innovations, validation and error propagation. *Chem. Geol.* **2006**, *233*, 185–195. [[CrossRef](#)]
22. Stone, J.; Allan, G.; Fifield, L.; Cresswell, R. Cosmogenic chlorine-36 from calcium spallation. *Geochim. Cosmochim. Acta* **1996**, *60*, 679–692. [[CrossRef](#)]
23. Ivy-Ochs, S.; Poschinger, A.; Synal, H.-A.; Maisch, M. Surface exposure dating of the Flims landslide, Graubünden, Switzerland. *Geomorphology* **2009**, *103*, 104–112. [[CrossRef](#)]
24. Zreda, M.G.; Phillips, F.M.; Elmore, D.; Kubik, P.W.; Sharma, P.; Dorn, R.I. Cosmogenic chlorine-36 production rates in terrestrial rocks. *Earth Planet. Sci. Lett.* **1991**, *105*, 94–109. [[CrossRef](#)]
25. Synal, H.-A.; Bonani, G.; Döbeli, M.; Ender, R.; Gartenmann, P.; Kubik, P.; Schnabel, C.; Suter, M. Status report of the PSI/ETH AMS facility. *Nucl. Instrum. Methods Phys. Res. Sect. B Beam Interact. Mater. Atoms* **1997**, *123*, 62–68. [[CrossRef](#)]
26. Christl, M.; Vockenhuber, C.; Kubik, P.; Wacker, L.; Lachner, J.; Alfimov, V.; Synal, H.-A. The ETH Zurich AMS facilities: Performance parameters and reference materials. *Nucl. Instrum. Methods Phys. Res. Sect. B Beam Interact. Mater. Atoms* **2013**, *294*, 29–38. [[CrossRef](#)]
27. Vockenhuber, C.; Miltenberger, K.-U.; Synal, H.-A.  $^{36}\text{Cl}$  measurements with a gas-filled magnet at 6 MV. *Nucl. Instrum. Nucl. Instrum. Methods Phys. Res. Sect. B Beam Interact. Mater. Atoms* **2019**, *455*, 190–194. [[CrossRef](#)]
28. Moore, A.K.; Granger, D.E. Calibration of the production rate of cosmogenic  $^{36}\text{Cl}$  from Fe. *Quat. Geochronol.* **2019**, *51*, 87–98. [[CrossRef](#)]
29. Stone, J.O.; Fifield, K.; Vasconcelos, P.M. Terrestrial Chlorine-36 Production from Spallation of Iron. In Proceedings of the 10th International Conference on Accelerator Mass Spectrometry, Berkeley, CA, USA, 5–10 September 2005.
30. Marrero, S.M.; Phillips, F.M.; Caffee, M.; Gosse, J.C. Corrigendum to “Cronus-Earth Cosmogenic  $^{36}\text{Cl}$  Calibration” [*Quat. Geochronol.* *31* (2016) 199–219]. *Quat. Geochronol.* **2021**, *61*, 101130. [[CrossRef](#)]
31. Leontaritis, A.D. The Late Quaternary Glacial History of Greece. Ph.D. Thesis, Harokopio University of Athens, Athens, Greece, 2021.
32. Moore, A. (Purdue University, West Lafayette, IN, USA). Personal communication, 2020.

33. Lal, D. Cosmic ray labeling of erosion surfaces: In situ nuclide production rates and erosion models. *Earth Planet. Sci. Lett.* **1991**, *104*, 424–439. [[CrossRef](#)]
34. Stone, J.O. Air pressure and cosmogenic isotope production. *J. Geophys. Res. Space Phys.* **2000**, *105*, 23753–23759. [[CrossRef](#)]
35. Licciardi, J.; Denoncourt, C.; Finkel, R. Cosmogenic <sup>36</sup>Cl production rates from Ca spallation in Iceland. *Earth Planet. Sci. Lett.* **2008**, *267*, 365–377. [[CrossRef](#)]
36. Reimer, P.J.; Austin, W.E.N.; Bard, E.; Bayliss, A.; Blackwell, P.G.; Ramsey, C.B.; Butzin, M.; Cheng, H.; Edwards, R.L.; Friedrich, M.; et al. The Intcal20 Northern Hemisphere Radiocarbon Age Calibration Curve (0–55 Cal Kbp). *Radiocarbon* **2020**, *62*, 725–757. [[CrossRef](#)]
37. Le Maitre, R.; Streckeisen, A.; Zanettin, B.; Le Bas, M.; Bonin, B.; Bateman, P. (Eds.) *Igneous Rocks: A Classification and Glossary of Terms: Recommendations of the International Union of Geological Sciences Subcommission on the Systematics of Igneous Rocks*, 2nd ed.; Cambridge University Press: Cambridge, UK, 2002.
38. Phillips, F.M.; Stone, W.D.; Fabryka-Martin, J.T. An improved approach to calculating low-energy cosmic-ray neutron fluxes near the land/atmosphere interface. *Chem. Geol.* **2001**, *175*, 689–701. [[CrossRef](#)]
39. Principato, S.M.; Geirsdóttir, Á.; Jóhannsdóttir, G.E.; Andrews, J.T. Late Quaternary Glacial and Deglacial History of Eastern Vestfirðir, Iceland Using Cosmogenic Isotope (<sup>36</sup>cl) Exposure Ages and Marine Cores. *J. Quat. Sci.* **2006**, *21*, 271–285. [[CrossRef](#)]